

## Propagation of Degradation-Induced Defects in Zeolitic Imidazolate Frameworks

Rebecca Han, Nina Tyminska, Jordan R. Schmidt, and David S. Sholl

*J. Phys. Chem. C*, **Just Accepted Manuscript** • DOI: 10.1021/acs.jpcc.9b00304 • Publication Date (Web): 26 Feb 2019

Downloaded from <http://pubs.acs.org> on February 27, 2019

### Just Accepted

“Just Accepted” manuscripts have been peer-reviewed and accepted for publication. They are posted online prior to technical editing, formatting for publication and author proofing. The American Chemical Society provides “Just Accepted” as a service to the research community to expedite the dissemination of scientific material as soon as possible after acceptance. “Just Accepted” manuscripts appear in full in PDF format accompanied by an HTML abstract. “Just Accepted” manuscripts have been fully peer reviewed, but should not be considered the official version of record. They are citable by the Digital Object Identifier (DOI®). “Just Accepted” is an optional service offered to authors. Therefore, the “Just Accepted” Web site may not include all articles that will be published in the journal. After a manuscript is technically edited and formatted, it will be removed from the “Just Accepted” Web site and published as an ASAP article. Note that technical editing may introduce minor changes to the manuscript text and/or graphics which could affect content, and all legal disclaimers and ethical guidelines that apply to the journal pertain. ACS cannot be held responsible for errors or consequences arising from the use of information contained in these “Just Accepted” manuscripts.



1  
2  
3  
4  
5  
6  
7  
8  
9  
10  
11  
12  
13  
14  
15  
16  
17  
18  
19  
20  
21  
22  
23  
24  
25  
26  
27  
28  
29  
30  
31  
32

# Propagation of Degradation-Induced Defects in Zeolitic Imidazolate Frameworks

33  
34  
35  
36  
37  
38  
39  
40  
41  
42  
43  
44  
45  
46  
47  
48  
49  
50  
51  
52  
53  
54  
55  
56  
57  
58  
59  
60

*Rebecca Han<sup>1</sup>, Nina Tyminska<sup>2</sup>, J.R. Schmidt<sup>2</sup>, David S. Sholl<sup>1\*</sup>*

<sup>1</sup>School of Chemical & Biomolecular Engineering, Georgia Institute of Technology, Atlanta,  
Georgia 30332-0100, United States

<sup>2</sup>Department of Chemistry, University of Wisconsin-Madison, Madison, WI, 53706, United  
States

## Corresponding author

\*david.sholl@chbe.gatech.edu, (p) 404-894-2822, (f) 404-894-2866

**ABSTRACT:**

Isolated defects induced by water and acid gases have been extensively characterized in ZIF-8, a prototypical metal-organic framework (MOF) material, but there is little understanding for how these single bond-breaking events lead to the structural amorphization observed after prolonged experimental exposure in acidic environments. We use Density Functional Theory calculations to provide the first analysis of defect propagation in a ZIF material. Given a single bond-breaking event (the first step in the formation of any defect state), we exhaustively explore the energetics of subsequent defect states and find strong preference for additional bond-breaking located adjacent to the previous defect in both two-defect and three-defect systems. This series of favorable reaction energies is more exothermic when we replace water with sulfuric acid as a protonating agent, in agreement with experimental observations that ZIF-8 degradation is accelerated in humid acid gas environments. To give initial insight into experimental signatures of defect propagation, we compare the simulated powder pattern in structures at varying levels of defect concentrations.

## 1. Introduction

Zeolitic imidazolate frameworks (ZIFs) are a subclass of crystalline porous adsorbents constructed from tetrahedrally coordinated Zn centers connected by imidazole-derived linkers, exhibiting a wide variety of accessible topologies, many of which are isomorphic to zeolites<sup>1</sup>. ZIFs have potential applications in chemical separations because they exhibit high thermal and chemical stability and have pore sizes comparable to small molecules<sup>2,3</sup>. However, like many other metal organic frameworks (MOFs)<sup>4</sup>, ZIFs are susceptible to degradation under humid and corrosive environments<sup>5</sup>. Understanding and controlling the degradation of new materials in complex environments is often a prerequisite to their successful implementation in practical applications<sup>6</sup>.

ZIF-8, one of the most well-studied ZIF structures, has 2-methylimidazole linkers and a sodalite (SOD) topology. ZIF-8 is considered to have robust hydrothermal stability<sup>7,8,9</sup>. Yaghi and co-workers<sup>7</sup> demonstrated that ZIF-8 retained crystallinity and porosity after being boiled in water and refluxing solvent for 7 days. Liu et al. showed that the selectivity and permeance of a ZIF-8 membrane remained constant for more than 40 days when left in atmospheric humidity<sup>10</sup>. However, recent experiments where ZIF-8 was contacted with pure water at room temperature revealed the release of Zn<sup>2+</sup> ions from the structure, implying hydrolysis of ZIF-8 occurs in aqueous solution at a rate proportional to the ZIF-8 to water ratio<sup>11,12</sup>. The ratio of crystal to water appears to dictate the rate and extent of dissolution of ZIF-8 and implies that previously observed water stability may have been a relative concentration effect; that is, exposure to sufficiently high relative concentration of pure water causes ZIF-8 to hydrolytically degrade.

It is widely hypothesized that degradation in MOFs and ZIFs begins with localized defect sites, in analogy to the highly reactive point defects in zeolites<sup>13</sup>. Existing modeling work on

1  
2  
3 formation of ZIF-8 defects has focused on point defects induced by humid or humid acid gas  
4 (CO<sub>2</sub>, SO<sub>2</sub>, NO<sub>x</sub>) environments<sup>14,15,16</sup>. Two types of defects, dangling linker (DL) and linker  
5  
6 (LV) defects<sup>15,17</sup>, were computationally proposed as the most likely isolated bond-  
7  
8 breaking events in ZIFs and have been experimentally observed with IR spectroscopy<sup>18</sup> and solid  
9  
10 state NMR<sup>19</sup>. The formation mechanisms attributed to these defects typically involve water or  
11  
12 hydrated species attacking and breaking the Zn-N coordination bond<sup>14</sup>. This local description of  
13  
14 defect formation, however, cannot fully describe the overall progression of material properties  
15  
16 observed experimentally<sup>17-20</sup>, where extended exposure to humid acid gases is found to  
17  
18 progressively amorphize the crystal structure and reduce the surface area of ZIF-8 and related  
19  
20 materials. Similar degradation is observed during aqueous exposure; aqueous SO<sub>2</sub> etches the  
21  
22 (110) surface of ZIF-8 preferentially<sup>21</sup> and completely amorphizes the structures after extended  
23  
24 exposures<sup>22</sup>. Interestingly, these processes are reversible upon appropriate post-treatment, an  
25  
26 observation that has allowed synthesis of ZIF materials that are not easy to produce by direct  
27  
28 synthesis<sup>23</sup>.  
29  
30  
31  
32  
33  
34

35 In this paper, we take an initial step towards bridging the gap between a microscopic  
36  
37 description of individual defects in ZIF-8 and the long-term degradation observed  
38  
39 experimentally. Specifically, we examine whether the existence of isolated defects in ZIF-8 can  
40  
41 promote further appearance of nearby defects. Our approach is motivated in part by previous  
42  
43 work on UiO-66, a MOF for which inclusion of defects has been extensively examined<sup>24</sup>. Prior  
44  
45 literature shows that UiO-66 can support multiple linker vacancy defects per twelve-coordinated  
46  
47 Zr center<sup>25</sup>. These defects occur during crystallization, and their concentration can be tuned in  
48  
49 synthesis by the addition of monocarboxylic acid modulators in varying proportions.  
50  
51 Furthermore, these defect inclusions tend to cluster in controllable ways<sup>26</sup>, analogous to the  
52  
53  
54  
55  
56  
57  
58  
59  
60

1  
2  
3 correlated Schottky vacancies that have been described<sup>27,28</sup> and computationally modeled<sup>29,30</sup> in  
4 various transition metal oxides. Computational models indicate that there is a smaller energetic  
5 penalty to form defects after removing three or four linkers per metal node, and solution-phase  
6 clustering of BDC molecules may further drive linker vacancies in the UiO-66 framework<sup>31</sup>.  
7  
8  
9

10  
11  
12 It is not clear *a priori* if clustering of defects in MOFs will generally be favorable. In the  
13 related area of radiation damage in solids, extensive studies have shown that the size of damage-  
14 induced defects follows a power law that declines steeply with increasing defect size<sup>32,33,34</sup>. This  
15 observation indicates that even events that locally inject enormous amounts (keV) of energy do  
16 not typically create a cascade of events leading to large defects. We acknowledge, however, that  
17 the analogy between these radiation damage events and degradation during long term exposure  
18 to reactive environments is imperfect. In the situation we envisage for MOFs the material is  
19 subjected to the possibility of many separate reactive events separated in time rather than the  
20 “short, sharp shock” of radiation damage.  
21  
22  
23  
24  
25  
26  
27  
28  
29  
30  
31  
32

33 In this work, we examine the hypothesis that defect propagation in ZIF-8 is promoted by  
34 the presence of existing defects. We showed previously that breaking a Zn-N bond in ZIF-8 is  
35 exothermic, and subsequently cleaving the second Zn-N bond to create a linker vacancy is even  
36 less energetically demanding<sup>15</sup>. Here, we investigate a prototypical defect propagation  
37 mechanism (using water to cleave the Zn-N bond), examining the dependence of the energy of  
38 formation of a second defect on its proximity of the first defect. In this case, we show that defect  
39 clustering is energetically favorable, that is, the presence of existing defects favors further defect  
40 formation. We then examine examples where H<sub>2</sub>SO<sub>4</sub> protonates the Zn-N bond and demonstrate  
41 that, in agreement with experimental observations, defect propagation is even more favorable in  
42 an acidic environment.  
43  
44  
45  
46  
47  
48  
49  
50  
51  
52  
53  
54  
55  
56  
57  
58  
59  
60

## 2. Computational Details

### 2.1. Density functional theory (DFT) calculations

Dispersion-corrected periodic density functional theory (DFT) calculations were performed using the Vienna Ab-initio Simulation Package (VASP) at the general gradient approximation (GGA) level<sup>35</sup>, using a restricted Kohn-Sham formalism with projector-augmented wave (PAW) method pseudopotentials and the Perdew-Burke-Ernzerhof (PBE) exchange-correlation functional combined with the DFT-D3 method of Grimme<sup>36</sup>. The ZIF-8 unit cell was obtained from the cubic crystal structure in the Cambridge Structural Database (CSD), which contains 276 atoms with lattice constant 16.99 Å. During geometry optimization of the pristine (defect-free) ZIF-8, both lattice parameters and ionic positions were fully relaxed using a conjugate gradient algorithm with a 600 eV plane wave energy cutoff until interionic forces were smaller than 0.01 eV/Å. The optimized lattice constant was 17.18 Å. The optimized unit cell structure was then used to construct models of the defect bulk ZIF-8. Lattice parameters were fixed in all the following energy-minimization calculations but atoms were relaxed until interionic forces were smaller than 0.01 eV/Å. A Gaussian smearing function of width 0.2 eV<sup>37</sup> was used to smear the electronic occupation around the Fermi level. The Brillouin zone was only sampled at the  $\Gamma$ -point for all calculations. VASP was used for all calculations involving fewer than 600 atoms.

To examine any possible finite size (i.e. concentration) effects, it was necessary to model defects in a 2×2×2 supercell of ZIF-8. The CP2K 4.1 code<sup>38</sup> with the Quickstep method<sup>39,40</sup> was used for these DFT supercell calculations on more than 600 atoms (Section 3.1.) because it is computationally more efficient than VASP. To verify the consistency between CP2K and VASP

1  
2  
3 results, identical  $1 \times 1 \times 2$  ZIF-8 lattices with and without defects were relaxed using both codes,  
4  
5 and the relative energy difference between the defect and defect free lattices were found to be in  
6  
7 good agreement;  $\Delta E_{\text{CP2K}} = 1.07$  eV and  $\Delta E_{\text{VASP}} = 1.08$  eV, respectively. Parameters for the  
8  
9 CP2K calculations were as follows: electronic energy was minimized until the convergence  
10  
11 criterion for the self-consistent field procedure ( $1.0 \times 10^{-7}$ ) was reached using a standard  
12  
13 diagonalization method (LAPACK) as implemented in CP2K; Goedecker-Teter-Hutter pseudo-  
14  
15 potentials<sup>41,42,43</sup> were used to treat nuclear and core electronic densities; and valence electrons  
16  
17 were represented by a mixed Gaussian (MOLOPT-DZVP)<sup>44</sup> and plane-wave (GPW)<sup>45</sup> (with a  
18  
19 cutoff of 600 Ry for the finest grid) basis set scheme.  
20  
21  
22

## 23 24 **2.2. X-ray diffraction (XRD) simulation**

25  
26 Simulated XRD patterns were calculated in Mercury<sup>46</sup> assuming a  $\text{CuK}\alpha$  radiation source  
27  
28 ( $\lambda = 1.54056$  Å) and symmetric pseudo-Voight peaks with  $0.05^\circ$  full width at half maximum.  
29  
30 Hydrogen atoms were assigned  $0.06$  Å<sup>2</sup> isotropic atomic displacements and all other atoms were  
31  
32 assigned  $0.05$  Å<sup>2</sup> displacements.  
33  
34  
35  
36  
37

## 38 **3. Results**

39  
40 To probe how bond-breaking reactions in ZIF-8 lead to structural degradation, we pose  
41  
42 three questions: (1) Does defect proximity influence the formation energy of subsequent defects?  
43  
44 (2) How does defect proximity vary spatially and chemically? (3) Can we extrapolate from what  
45  
46 we learn about defect proximity preference to explain degradation in complex environments on  
47  
48 long timescales?  
49  
50

51  
52 We start with the simplest model of a defect formation event: water-induced cleavage of  
53  
54 the Zn-N bond in ZIF-8. The defect formation energy,  $\Delta E$ , is defined as  
55  
56  
57  
58  
59  
60

$$\Delta E = E_{\text{defect ZIF}} - E_{\text{pristine ZIF}} - E_{\text{H}_2\text{O}} \quad (1)$$

where  $E_{\text{defect ZIF}}$ ,  $E_{\text{pristine ZIF}}$ , and  $E_{\text{H}_2\text{O}}$  are the energies of a ZIF structure containing the defect, a defect-free ZIF structure, and an isolated water molecule, respectively. A negative value of  $\Delta E$  denotes an exothermic reaction. Defect models were constructed in a periodic ZIF-8 unit cell and calculations were performed using the VASP software as described in Section 2.1.

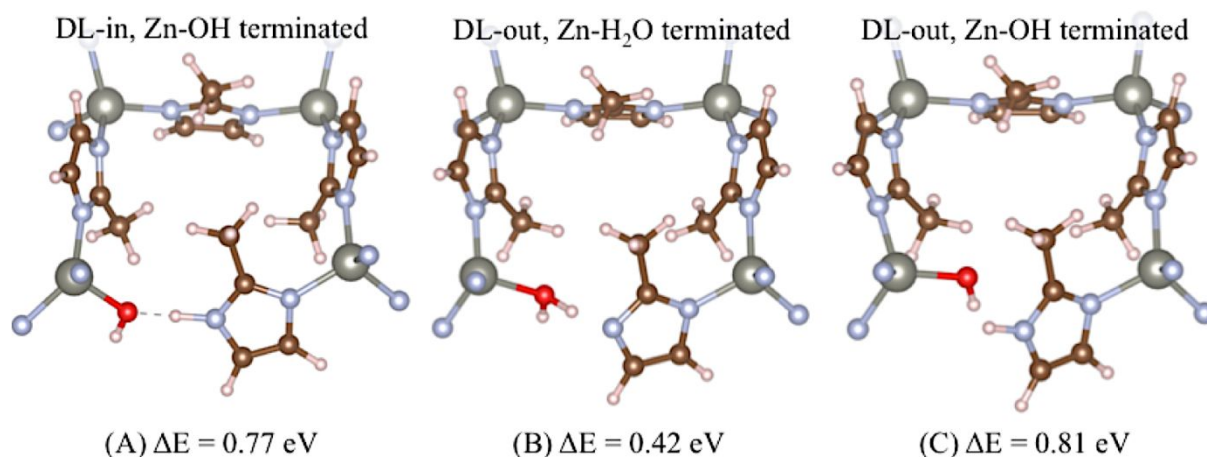


**Figure 1.** Three configurations for an isolated water-induced dangling linker (DL) defect in ZIF-8, and their associated formation energies: DL-in (A) versus DL-out (B, C) and metal terminations Zn-OH (A, C) versus Zn-H<sub>2</sub>O (B). The two Zn terminations represent two different reactions, separated by proton transfer. This figure and all subsequent molecular structures were produced using VESTA<sup>47</sup>.

Breaking a single Zn-N bond in ZIF-8 creates a dangling linker (DL) defect<sup>14,15,17</sup>. This defect can take several distinct forms, depending on the conformation of the dangling linker and termination of the open metal site. In what we denote as the DL-in conformation (Fig. 1, A), the linker remains in the original Zn-Imidazole-Zn plane, and the Zn-Zn distance increases from 6.0 Å to 7.9 Å. In what we denote the DL-out conformation (Fig. 1, B and C), the Zn-Zn distance is closer to 7.0 Å, and the imidazole swings approximately 30° out of the plane. For each of these two conformations, we also need to consider whether the attacking water molecule adsorbs at the newly created open metal site (Fig. 1, B), or whether it adsorbs and transfers a proton to the

1  
2  
3 dangling imidazole while the remaining hydroxyl terminates the Zn (Fig. 1, A and C). All of the  
4 accessible DL states and their associated formation energies are summarized in Figure 1, and we  
5  
6  
7 will refer to these variations of a single DL defects as A, B, or C type defects. These energies are  
8  
9  
10 comparable with the single dangling linker formation energy of 0.51 eV calculated by Zhang et  
11  
12 al.<sup>14</sup>, although we point out the different lattice constant and zero damping DFT-D3 correction  
13  
14 (as opposed to Becke-Johnson damping) used in this study. While the previous work constructed  
15  
16 a representative dangling linker defect, we explicitly constructed distinct defect structures with  
17  
18 dramatically different local geometries (DL-in versus DL-out) and proton transfer chemistry (Zn-  
19  
20 OH versus Zn-H<sub>2</sub>O) in order to sample conformation space. We also performed calculations  
21  
22 probing the existence of a DL-in, Zn-H<sub>2</sub>O terminated defect but in all cases these structures  
23  
24 spontaneously relaxed into the more favorable DL-in, Zn-OH state. Termination has more impact  
25  
26 than conformation on formation energy of the first defect; B is more favorable than A or C by  
27  
28 ~0.35 eV, while A is only 0.04 eV more favored than C. If only an isolated defect forms, we  
29  
30 expect the most energetically stable state B to dominate. With additional DL defects, we can ask  
31  
32 if B will always form or if the relative stability of the defects is influenced by their local defect  
33  
34 environment – this question is addressed in Section 3.2.  
35  
36  
37  
38  
39  
40  
41  
42  
43  
44  
45  
46  
47  
48  
49  
50  
51  
52  
53  
54  
55  
56  
57  
58  
59  
60

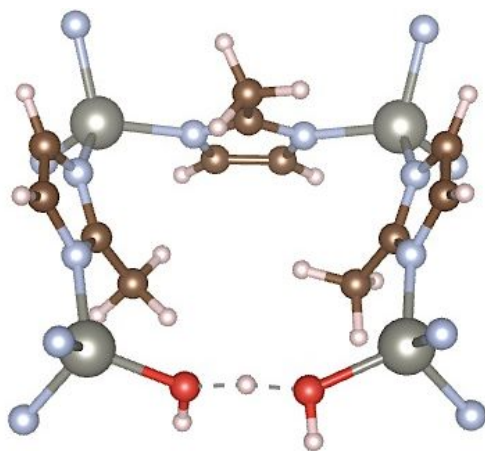


**Figure 2.** A linker vacancy (LV) defect formed by two successive bond-breaking events involving two water molecules. Once both Zn-N bonds attaching a linker to the ZIF-8 framework are hydrolyzed, the liberated imidazole is protonated by one of the water molecules, and the open Zn sites are terminated by hydrogen-bonded water and hydroxyl.

While there are many possible conformations for a dangling linker (DL) defect, there is only one defect state for a linker vacancy (LV) defect, shown in Figure 2. Two Zn-N water-induced bond-breaking events are required to form this defect. After one of the water molecules donates an H atom to protonate the liberated imidazole, the remaining OH and H<sub>2</sub>O hydrogen bond. The linker vacancy formation energy is given as

$$\Delta E_{1LV} = E_{1LV} + E_{HL} - E_{\text{pristine ZIF8}} - 2E_{\text{H}_2\text{O}} = 0.57 \text{ eV.} \quad (2)$$

where  $E_{1LV}$  is the energy of a ZIF structure containing a single linker vacancy defect, and  $E_{HL}$  is the energy of an isolated protonated imidazole molecule. Again, this energy is comparable to the single linker vacancy formation energy 0.62 eV calculated by Zhang et al.<sup>14</sup> We can also think of the LV defect as the sum of two successive Zn-N bond-breaking events on either end of an imidazole linker. Recall that proton transfer is most important distinction for the reaction energy of breaking a single Zn-N bond to form a DL defect. It follows that one of the bond-breaking events required for LV formation involves proton transfer and the other does not; order does not matter because there is a unique product state. We can compare the energy of the linker vacancy to the energies of two isolated dangling linker defects (denoted  $E_{1DL,A}$  or  $E_{1DL,B}$ ) as follows

$$E_{1LV} + E_{HL} + E_{\text{pristine ZIF8}} - E_{1DL,A} - E_{1DL,B} = -0.62 \text{ eV.} \quad (3)$$

Since the energy difference between the A and B states was 0.35 eV, it is 0.27 eV more exothermic to form a LV defect than to form two infinitely separated DL defects. If we assume that the linker remains in the pore rather than being removed, as has been recently suggested<sup>16</sup>, it is still 0.11 eV more favorable (the  $E_{HL}$  term is dropped in Equation 3) to form the LV defect

1  
2  
3 than to form two infinitely separated DL defects. This suggests that breaking two nearby bonds is  
4 energetically favorable, an observation we examine further in the following section.  
5  
6

### 7 **3.1. Clustered defects are energetically preferred in ZIF-8**

8  
9  
10 The energy required to form a second defect located far in the bulk from a first defect is  
11 necessarily independent of the first defect's formation energy. Therefore, preference for or  
12 against the formation of additional defects can only be relevant within some distance from an  
13 existing defect. Here, we investigate whether proximity is favorable or unfavorable to subsequent  
14 defect formation in ZIF-8 and we establish the distance threshold at which the formation of a  
15 second defect becomes energetically independent from the first.  
16  
17  
18  
19  
20  
21  
22

23  
24 Since the linker vacancy is well-defined (it only has one conformation) and already  
25 represents a more clustered state than the single bond-breaking event, we can simplify the  
26 number of conformations we have to consider by considering the proximity between two linker  
27 vacancy defects. This is quantified by measuring the Zn-Zn distance between two OH-terminated  
28 metal centers. Given this definition, the closest possible defects are adjacent; two of the four  
29 imidazoles to which any one metal center is tetrahedrally coordinated are removed, creating two  
30 adjacent linker vacancies that share a Zn vertex. This situation is illustrated in Figure 3. To  
31 examine a range of defect separation distances, we constructed a  $2 \times 2 \times 2$  supercell. Within this  
32 computational volume, the farthest unique Zn-Zn separation attainable while considering  
33 periodic images is  $\sim 25$  Å. We built a series of defect systems with two LVs separated by 0,  $\sim 6$ ,  
34  $\sim 14$ ,  $\sim 20$ , and  $\sim 25$  Å (see Figure 3), which is equivalent to a second LV located 0, 1, 2, 3, or 4  
35 linkers away from the first LV. Formation energies for the 2LV systems ( $\Delta E_{2LV}$ ) and the infinite  
36 separation reference ( $\Delta E_{2LV, \infty}$ ) are defined as follows:  
37  
38  
39  
40  
41  
42  
43  
44  
45  
46  
47  
48  
49  
50  
51  
52

$$53 \Delta E_{2LV} = E_{ZIF, 2LV} + 2E_{HL} - E_{ZIF (2 \times 2 \times 2)} - 4E_{H2O} \quad (4)$$

54  $\Delta E_{2LV, \infty}$

1  
2  
3 Structures with LVs separated by 0 and  $\sim 6$  Å were constructed in  $1 \times 1 \times 2$  supercells and  
4 relaxed in CP2K and VASP to ascertain good agreement between the calculation methods (see  
5 relaxed in CP2K and VASP to ascertain good agreement between the calculation methods (see  
6 Section 2.1.). The optimized LV pairs were then placed into  $2 \times 2 \times 2$  supercells, and additional  
7  $2 \times 2 \times 2$  supercells were constructed for LV pairs separated by  $\sim 14$ ,  $\sim 20$  and  $\sim 25$  Å. CP2K was  
8 used to relax this set of  $2 \times 2 \times 2$  systems and calculate the LV pair formation energies. It is evident  
9 from Figure 4 that forming two defects close together (within  $\sim 14$  Å) is considerably more  
10 favorable than forming isolated defects. Adjacent LVs sharing a Zn vertex (Zn-Zn = 0 Å) require  
11 0.2 eV less energy to form than the infinite separation reference state. More than half this energy,  
12 about 0.14 eV, is associated with placing the second defect just one linker away ( $\sim 6$  Å). This  
13 indicates a strong preference for adjacent clustering of two linker vacancy defects.

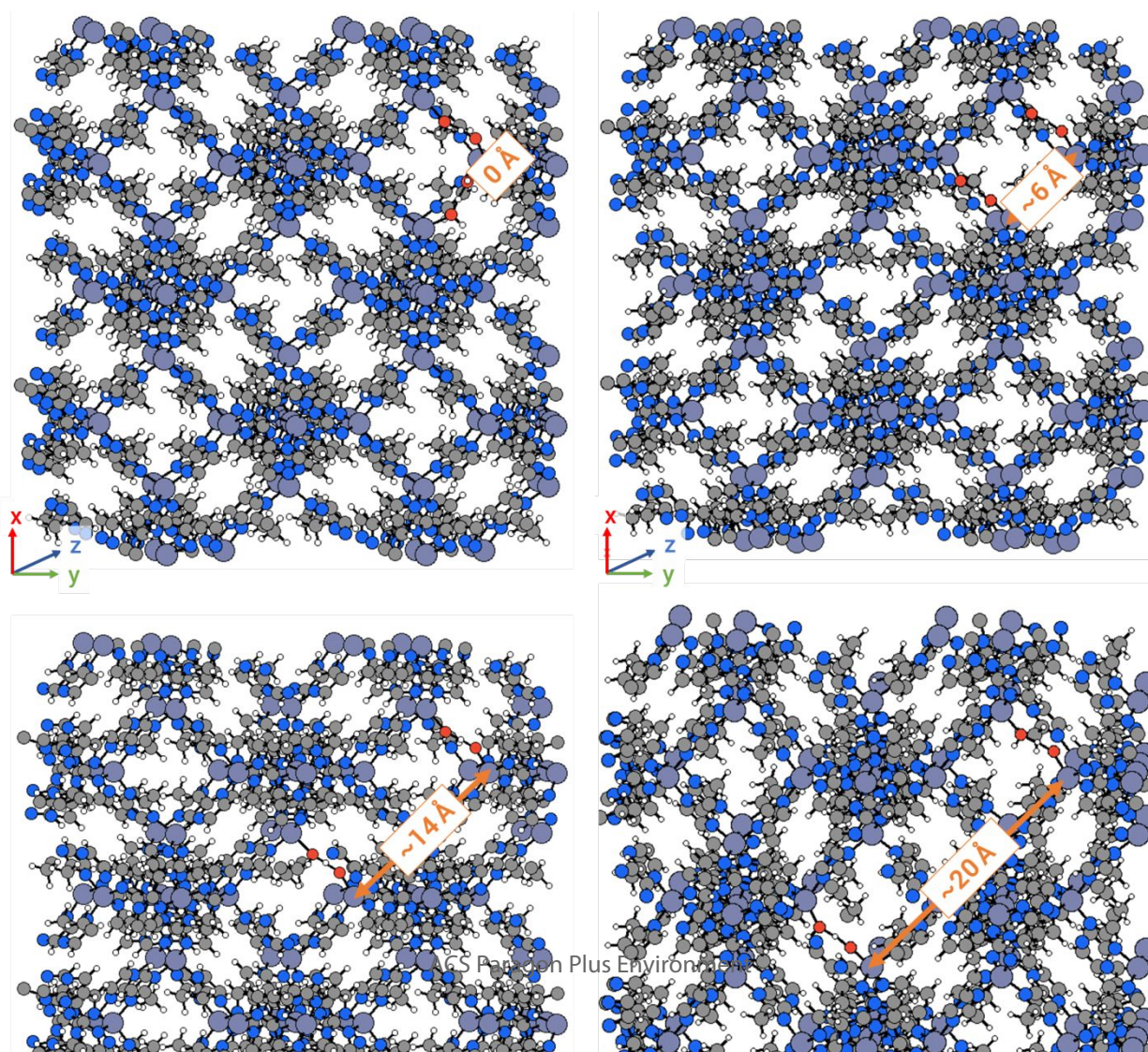


**Figure 3.** Two linker vacancy defects constructed in a  $2\times 2\times 2$  periodic supercell of ZIF-8 and separated by 0 Å (top left),  $\sim 6$  Å (top right),  $\sim 14$  Å (bottom left),  $\sim 20$  Å (bottom right). These four states have the second linker vacancy located 0, 1, 2, or 3 linkers away from the first defect, respectively.

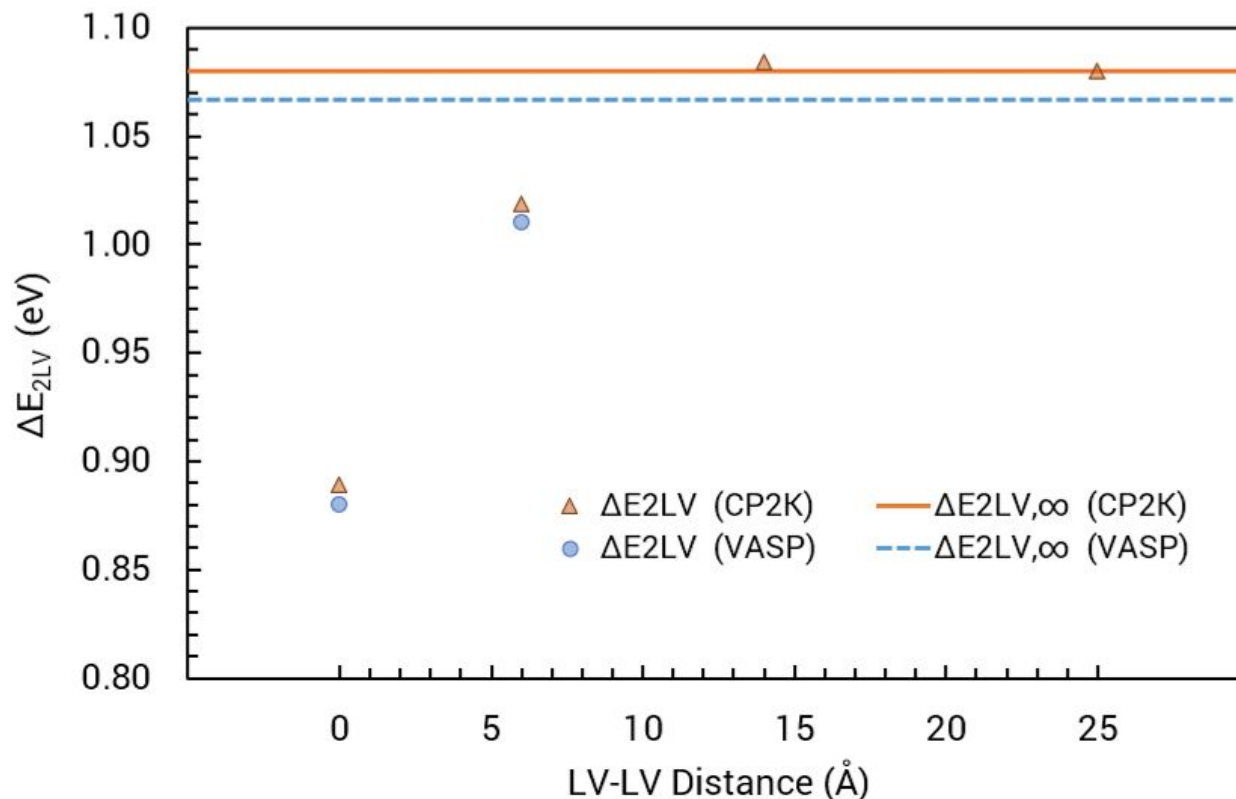


**Figure 4.** Formation energy of a second linker vacancy (LV) defect plotted as a function of its spatial separation from the first LV defect (discrete points), along with the infinite separation reference (horizontal lines). There is good agreement between formation energies calculated using CP2K and VASP. Numerical data given in Table S1.

### 3.2. Predicting the likeliest defect pair states

The results above indicate that clustering of LV defects in ZIF-8 is energetically preferred. This motivated us to systematically investigate possible ways to form a second nearby defect and predict the most favorable defect pair states. We already established that at separations beyond 14 Å forming a second LV is energetically independent of the first LV defect, so it is sufficient to consider defect pairs in a single ZIF-8 unit cell with lattice constant  $\sim 17$  Å. This system size means we could calculate formation energies using VASP, as detailed in Section 2.1.

Formation of an initial defect by breaking the first Zn-N bond was thoroughly considered above in terms of the possible conformations and terminations (see Figure 1). Termination was the most important factor, leading to our identification of an A and B type DL defect representing Zn-OH and Zn-H<sub>2</sub>O termination, respectively. Now we ask which bond is most favored to break *next*, after initial defect formation. To answer this question, we have several new considerations. First, the second defect can create a linker vacancy (LV), or it can create a second dangling linker (DL). In the latter case, we also need to examine which dangling linker pair states are most stable. We will further demonstrate at the end of this section that it can be more favorable to create a second dangling linker than to form the linker vacancy.

The remaining considerations in forming a second DL defect have to do with orientation and location. Since the imidazole is only cleaved on one side, there are naturally two “ends” of the dangling linker defect – the terminated Zn and the dangling linker. Figure 5 illustrates two possible ways to orient a new dangling linker with respect to the first, either with the two terminated ends sharing a Zn vertex (LXXL orientation) or the dangling linker of one defect closer to the terminated Zn of the other defect (LXLX orientation).

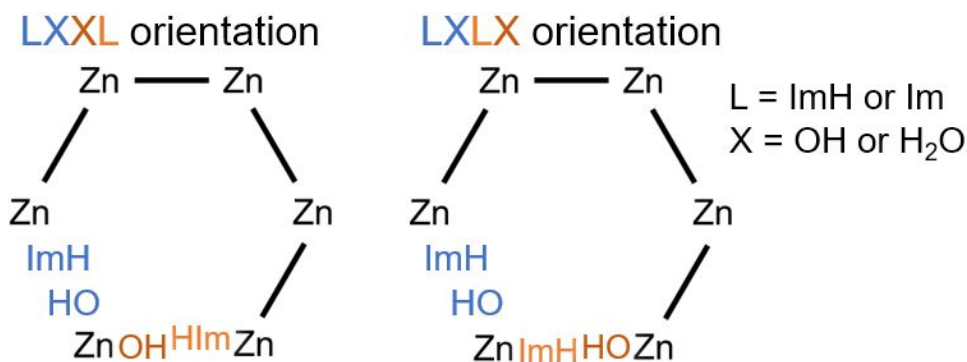


**Figure 5.** The 6-member ring ZIF-8 can be represented by a simplified schematic where the Zn nodes are connected by imidazoles represented as straight lines (black). Water-induced dangling linker (DL) defects are shown as Zn-ImH and OH-Zn. The two rings represent two ways to orient a second DL defect (orange) adjacent to a first defect (blue); the Zn-OH terminated ends can be closest (LXXL orientation) or the dangling Zn-ImH end can be closer to a Zn-OH terminated end (LXLX orientation).

Two additional considerations pertain to the location of the second DL defects, namely adjacency and inclusion in the same ring. Figure 6 shows four combinations of these variations represented in a simplified cartoon of the sodalite (SOD) cage. A single SOD cage is composed of 24 metal nodes and 36 linkers, but the  $1\times 1\times 1$  unit cell of ZIF-8 only contains 12 unique metal nodes (labelled A-L) and 24 unique linkers, shown as the grey Zn atoms and linkers in Figure 6, respectively. This implies that the SOD cage spans neighboring periodic images of the SOD unit cell, shown as blue Zn atoms and linkers. Therefore, when identifying all the unique Zn-Im-Zn pairs that can form DL defects, a closer site may be contained in a periodic image. Given a first DL defect (highlighted in cyan), the second DL defect (highlighted in orange) can be adjacent (“2DL adj”) or separated (“2DL away”). There is additional variation depending on whether both defects are in the same ring, and the size of the ring. ZIF-8 only has 4-member (4M) and 6-member (6M) rings – “adj” defects can either share a 4M ring (Figure 6, bottom left) or a 6M ring (top left), and “away” defects can share a 4M ring, a 6M ring (top right), or no ring (bottom right, labelled “xN”).

Accounting for all the possible combinations of forming a second DL defect given an initial A or B type DL, we built an exhaustive list of thirty-two defect pairs possible in a  $1\times 1\times 1$  unit cell and calculated the energy of each system. These energies are listed in Table S2 and the corresponding converged structures are provided in the Supplementary Information. Blank entries in Table S2 indicate that a defect state spontaneously relaxed into one of the others.

The results in Table S2 show that adjacent, co-terminal DL defect pairs were most favorable. This agrees with the trend we observed for a pair of linker vacancy defects in Figure 4. By comparing the optimized final geometries of defect structures, we find that conformations

with bond angles closest to the ideal tetrahedral bonding angle of  $109.5^\circ$  are more stable. More hydrogen bonding also increases stability, which explains the preference for co-terminal defects over adjacent defects oriented with one terminated end closer to one dangling linker end.

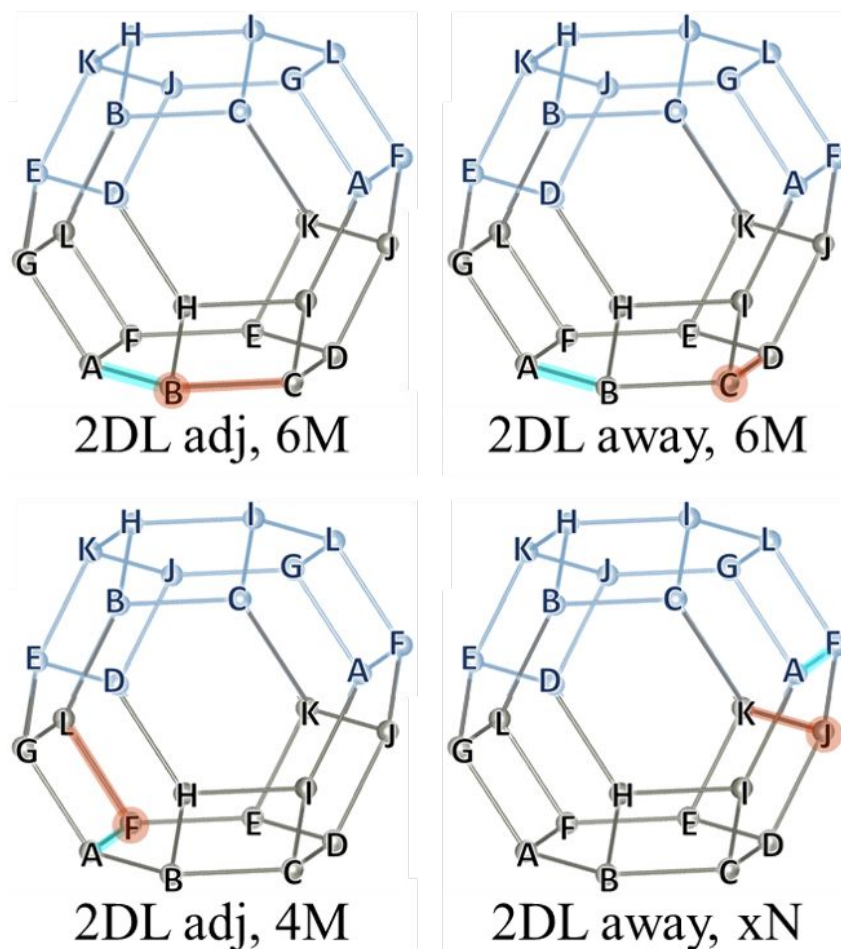


**Figure 6.** A simplified schematic of the ZIF-8 SOD cage is shown where Zn atoms (labelled with letters A-L) are connected by imidazoles (represented as straight lines). Zn atoms and imidazoles within a  $1 \times 1 \times 1$  unit cell of ZIF-8 are grey, while nodes and linkers from neighboring periodic images are blue. Given a first dangling linker (DL) defect highlighted in cyan, there are multiple choices to place a second DL defect highlighted in orange: the two defects can be adjacent (“2DL adj”) or separated (“2DL away”), and they can either share a ring (“4M” or “6M”) or not (“xN”).

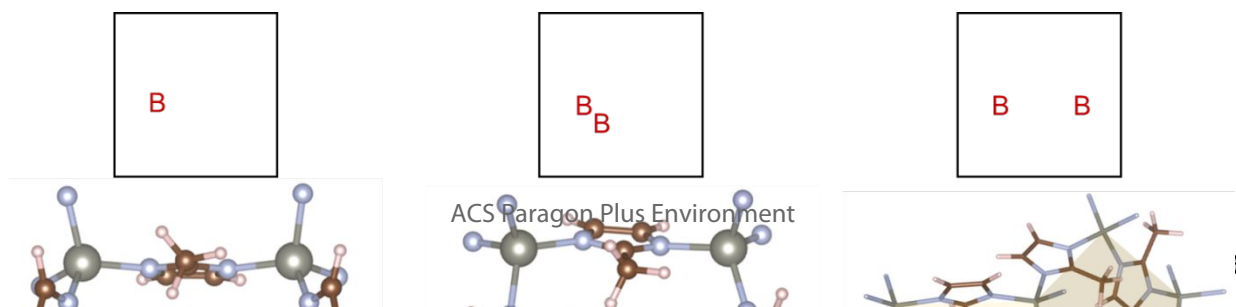
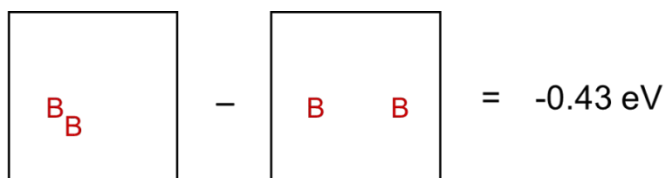


**Figure 7.** All three defects shown here are Zn-OH terminated (type B). From left to right, they are the optimized structures of the first defect B, the adjacent defect pair B<sub>2</sub>, and a pair of defects 2B separated by one linker which do not share a ring (“away, xN” in the previously defined terminology).

Based on the above observations, we know the most energetically favorable DL pairs will have adjacent, co-terminal defects. To quantify how much more energetically favorable these systems are compared to other types of defect pairs, we can simplify our description of each defect state using a combination of A and B type dangling linkers. Since the B dangling linker was favored for the first defect, we started by considering the complex defect configurations for a pair of type B defects. Figure 7 shows the single defect (left), a pair of adjacent co-terminal defects B<sub>2</sub> (middle), and a pair of separated defects 2B (right). We can therefore introduce the site-vacancy notation in Figure 7 to indicate possible arrangements in a 1×1×1 unit cell. The energy differences for several scenarios of interest can be summarized using this notation as in Figure 8.

The results for a pair of Type B defects are shown in Figure 8. There is a 0.43 eV energetic penalty associated with forming the second defect even one linker’s distance away from the first (the 2B state) instead of adjacent to the first (the B<sub>2</sub> state). Slightly more energy is required to separate a defect pair by an infinite distance (the 2(B) state, which, by definition, requires twice the formation energy of the single type B defect to form). This penalty is 0.59 eV if we start from the adjacent pair, or 0.16 eV if we start with the pair separated by one linker’s distance. These results indicate clear preference for a second type B defect to form in a co-terminal orientation at an adjacent location to the first. That is, the answer to the Shakespearean question “2B or not 2B?” is, at least in terms of energy preference, “not 2B”.



$$B_2 - 2B = -0.43 \text{ eV}$$

1  
2  
3 **Figure 8.** Site-vacancy notation describing the energetics of separating a pair of clustered type B defects (top),  
4 removing one of a pair of clustered defects infinitely far away (middle), or removing one of a pair of separated  
5 defects infinitely far away (bottom). Each black square represents a single ZIF-8 unit cell with periodic boundary  
6 conditions. The energies are all exothermic, indicating a preference for clustering.  
7

8 We can also examine defect pairs containing type A defects. For a pair of type A defects,  
9 the  $A_2$ ,  $2A$ , and  $2(A)$  states are defined in the same way as the  $B_2$ ,  $2B$ , and  $2(B)$  states. For a  
10 mixed pair of type A and B defects, we define the AB state as a pair of adjacent, co-terminally A  
11 and B defects, the A\_B state as a pair of A and B defects separated by one linker's distance, and  
12 the A+B state as an infinitely separated pair of A and B defects. Site vacancy descriptions similar  
13 to Figure 8 for the A only pair and mixed AB pair are included Figures S1 and S2.  
14  
15  
16  
17  
18  
19  
20  
21

22 Figure 9 compares the formation energies for all single and pair defect states discussed  
23 thus far. There are two main conclusions. First, as we already stated, B has the lowest single  
24 defect formation energy (compared to the other single defect states A and C) and therefore we  
25 expect that the first defect to form will be type B. However, when we add a defect, having two A  
26 defects adjacent and co-terminal is the most favorable pair defect state – the  $A_2$  defect shown in  
27 Figure 9 (inset) has the lowest formation energy among all single and pair defects, although the  
28  $B_2$  state has a comparable formation energy. It is surprising and significant that the clustered  
29 defect pair is more stable than the single defect system, indicating that the energy gain from  
30 clustering is larger in magnitude than the single defect formation energy.  
31  
32  
33  
34  
35  
36  
37  
38  
39  
40  
41  
42  
43  
44  
45  
46  
47  
48  
49  
50  
51  
52  
53  
54  
55  
56  
57  
58  
59  
60

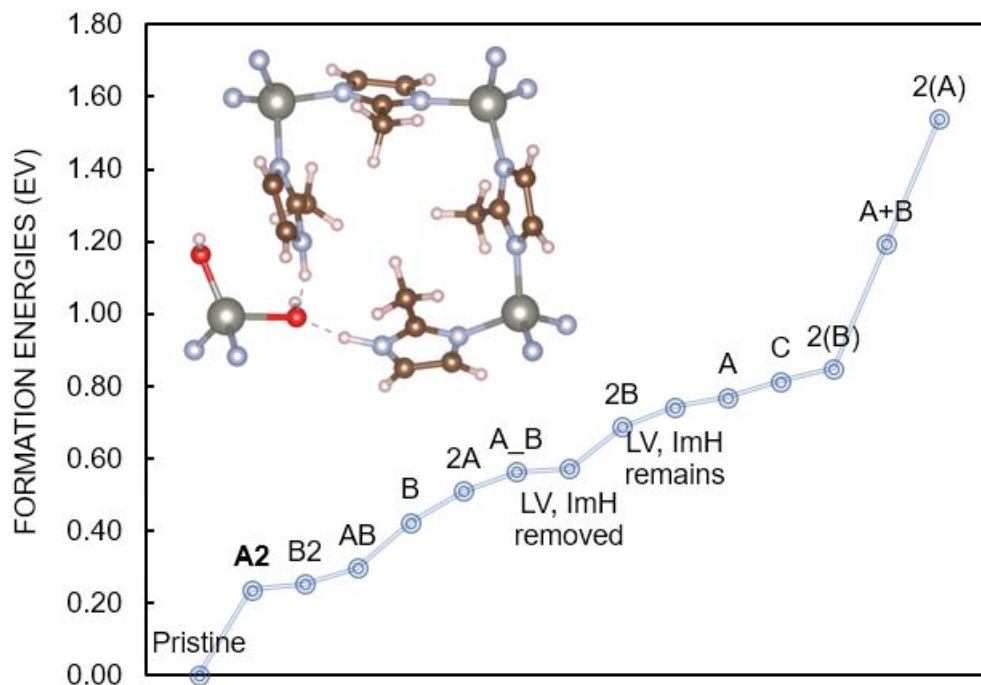


**Figure 9.** Formation energies of ZIF-8 systems with no defects, single defects, and defect pairs. The  $A_2$  defect pair is the most stable configuration and its geometry is shown in the inset. The  $A_2$ ,  $B_2$ , and  $AB$  defect pairs are oriented co-terminally and located adjacent to one another. The  $2A$ ,  $2B$ , and  $A_B$  defect pairs are located one linker's distance apart. The  $2(A)$ ,  $2(B)$ , and  $A+B$  defect pairs are located infinitely far away from one another. We also considered both linker vacancy defects where the freed linker remains near the pore window (ImH remains), and where it has diffused away (ImH removed). Energies are given in Table S2 of the SI.

To understand why the less favorable single defect  $A$  suddenly becomes more favorable when a second, adjacent  $A$  defect is introduced, we posit that the dangling linker formation energy can be split into the sum of an intrinsic energy cost to hydrolyze a  $Zn-N$  bond,  $\epsilon$ , plus a “strain” cost of the surrounding framework distorting to accommodate the dangling linker,  $\sigma$ . Therefore, for the first defect:

$$\Delta E_{1DL} = E_{\text{defect ZIF}} - E_{\text{pristine ZIF}} - E_{H_2O} = \epsilon + \sigma \quad (6)$$

If forming a second adjacent dangling linker can relieve the strain cost fully by introducing more flexibility into the larger defect site, the overall energy required to introduce two dangling linkers would be double the intrinsic energy cost:

$$\Delta E_{2DL} \approx 2\epsilon \quad (7)$$

In this description, the intrinsic energy cost is assumed to be approximately independent of conformation since it only depends on the nature of the Zn-N bond being broken. If this simple description is valid, the difference in energy cost to form A, B, and C type defects should be entirely explained by the strain cost, which is alleviated in the subsequent A<sub>2</sub>, B<sub>2</sub>, and C<sub>2</sub> defects, respectively. We independently estimated  $\epsilon$  and  $\sigma$  from the formation energies for single and pair defect states, giving the results in Table 1. These results show that the intrinsic energy cost is consistently  $\sim 0.13$  eV, with significantly more variation in the strain cost for the three defect types. This approximate analysis strongly suggests that propagation of bond-breaking defects is favorable when clustering of defects creates conformations where framework strain is alleviated. This observation may be useful in considering the potential clustering of defects in a much broader range of MOFs than the single example of ZIF-8 that we have considered here.

**Table 1.** Formation energies (all in eV) of single and pair dangling linker defect states, decomposed into the sum of the intrinsic energy cost  $\epsilon$  to hydrolyze a Zn-N bond and the strain cost  $\sigma$  of accommodating framework deformation due to the dangling linker.

Defect	$\Delta E_D = \epsilon + \sigma$	$\Delta E_{D2} = 2\epsilon$	$\epsilon$	$\sigma$
A	0.77	0.24	0.12	0.65
B	0.42	0.25	0.13	0.30
C	0.81	0.25	0.13	0.69

### 3.3. Acid gas hydrolyzed defect pairs

Previous work has demonstrated that ZIF-8 degrades readily upon exposure to humid SO<sub>2</sub> and DFT calculations supported the conclusion that energetics of defect formation were significantly more favorable with H<sub>2</sub>SO<sub>4</sub> (rather than H<sub>2</sub>O) as the protonating species<sup>17</sup>. Here we extend that analysis by examining pairs of defects, replacing H<sub>2</sub>O with H<sub>2</sub>SO<sub>4</sub> as the acid. Based on the previous definitions of an A and B type single DL defect, depending on whether a proton

is transferred from the acid to the dangling imidazole linker, we can similarly define an  $\alpha$  and  $\beta$  structure for the first  $\text{H}_2\text{SO}_4$  defect as shown in

Figure 10. The formation energy of this first defect is given as

$$\Delta E_{1\text{DL}, \text{H}_2\text{SO}_4} = E_{\text{defect ZIF}} - E_{\text{pristine ZIF}} - E_{\text{H}_2\text{SO}_4} \quad (8)$$

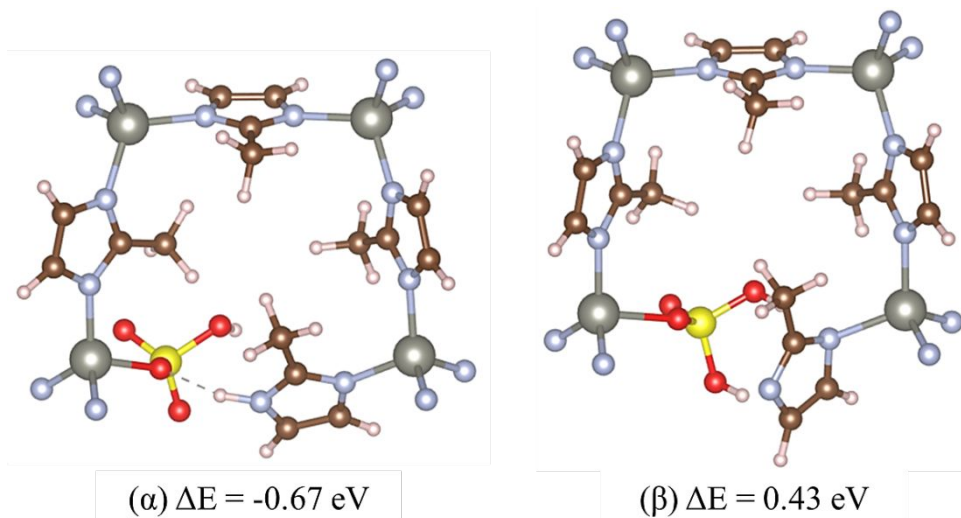


**Figure 10.** Single dangling linker defect states  $\alpha$  and  $\beta$  for  $\text{H}_2\text{SO}_4$ -induced defects. The  $\alpha$  state with proton transfer is exothermic while the  $\beta$  state is not.

Unlike the single water-induced defect, the  $\alpha$  state where sulfuric acid transfers a proton to the dangling imidazole linker is preferred; the  $\beta$  state has a non-spontaneous formation energy (see Figure 10). This is likely due to the higher Bronsted acidity of sulfuric acid than water, making proton transfer much more favorable. Based on our previous defect pair calculations involving water, we focus on the  $A_2$  and  $AB$  states with  $\text{H}_2\text{SO}_4$  as the degradation agent. We consider systems where one or both water molecules are replaced by sulfuric acid, the  $\alpha A$  and  $\alpha B$  states or the  $\alpha_2$  and  $\alpha\beta$  states, respectively. The reaction energy for these four defect pair

states  $\alpha D$  ( $D = \alpha, \beta, A, \text{ or } B$ ) are calculated as shown in Equation 9-10, where  $\Delta\Delta E_{\alpha D}$  compares the change in energy of replacing water with sulfuric acid in an otherwise identical reaction.

$$\Delta E_{\alpha D} = E_{\alpha D} + E_{\text{pristine ZIF}} - E_{\alpha} - E_D \quad (9)$$

$$\Delta\Delta E_{\alpha D} = \Delta E_{\alpha D} - \Delta E_{AD} \quad (10)$$

When only one water is substituted with  $\text{H}_2\text{SO}_4$ , the reaction energies are significantly more exothermic than the defect pair reaction energies with only water:  $\Delta\Delta E_{\alpha A} = -0.55$  eV and  $\Delta\Delta E_{\alpha B} = -0.97$  eV. This agrees with previous work<sup>17</sup> that degradation in ZIF-8 is accelerated by humid  $\text{SO}_2$ . However, when both water molecules are replaced with sulfuric acid, the reaction energies are no longer significantly more exothermic than the  $\text{H}_2\text{O}$  pair defects,  $\Delta\Delta E_{\alpha_2} = -0.08$  eV and  $\Delta\Delta E_{\alpha\beta} = 0.52$  eV. This may be due to steric reasons,  $\text{H}_2\text{SO}_4$  is a larger molecule than  $\text{H}_2\text{O}$ , or it may indicate that the presence of water is necessary to creating a favorable  $\alpha A$  or  $\alpha B$  intermediate state.

### 3.4. Thermodynamics of additional defect propagation

Having thoroughly considered the relative formation energy for defect pairs, we now want to determine whether it is energetically preferable to introduce a third DL adjacent to pre-existing defects or some distance away from them. The combinations of possible triplet defect states are too extensive to be exhaustively explored. Instead, we show four sample triplet defect states in **Error! Reference source not found.** with the corresponding defect formation energies (referenced to energy of pristine ZIF-8 and three isolated water molecules) shown in comparison to the defect pair formation energies in Figure 12. Two of these defect triplets (States III and IV in Fig. 11) have lower formation energy than any other defect state we have examined. Some of this energetic gain from additional clustering may be due to finite size effects as we add more and more defects into a unit cell simulation model. Nevertheless, the existence of these energy

downhill states suggests that adding multiple defects can reduce the overall formation energy of the system, leading to spontaneous defect propagation. It is interesting to note that the most preferred configurations for three DL defects are to share a 6M ring while for DL pairs, defects located adjacent and co-terminal in the same 4M ring were preferred. We attribute this to the increased strain cost of adding a third DL in the same 4M ring, which is less pronounced in the same 6M ring because the larger ring has more flexibility to accommodate the defects.

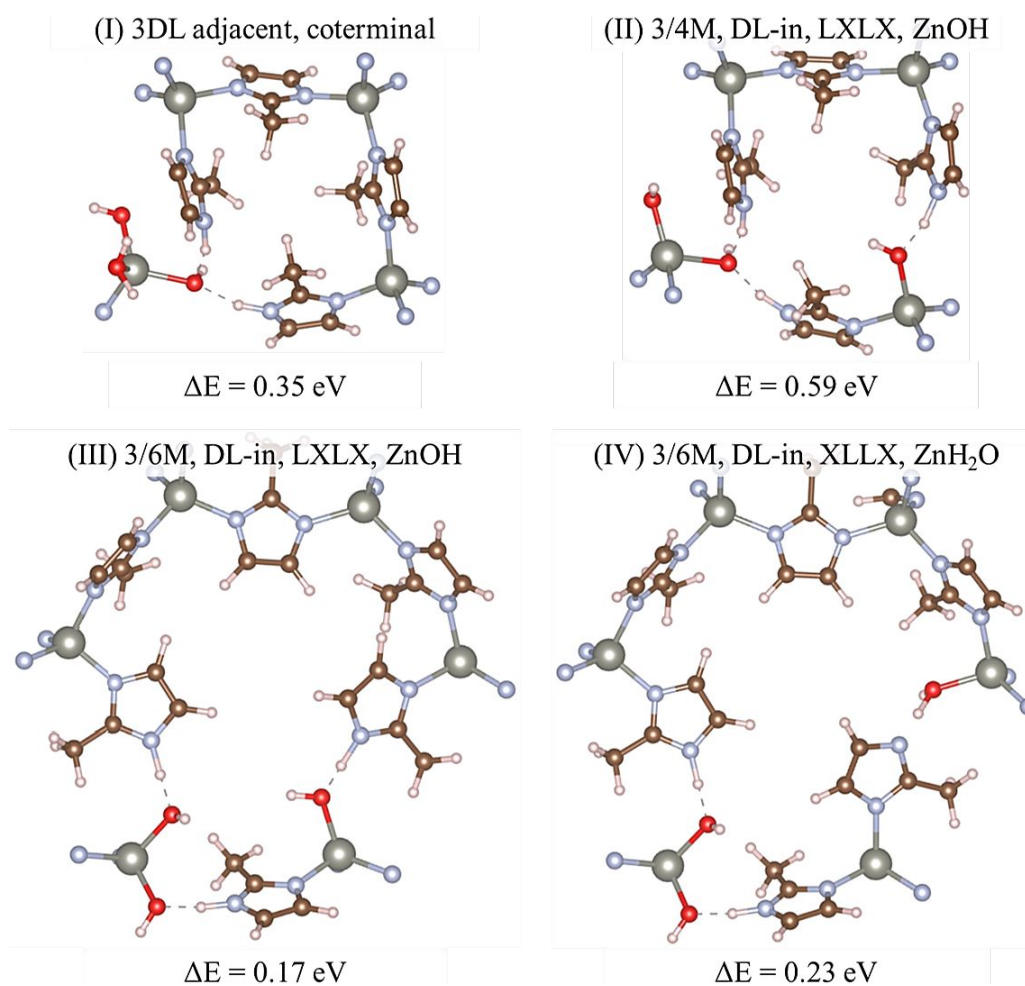


**Figure 11.** Four examples of triple defect states where water hydrolyzes three Zn-N bonds in each system to form three dangling linker defects. The three defects can be located, relative to one another, adjacent and co-terminal (I), sequentially around the same 4M ring (II), or sequentially around the same 6M ring (III and IV).

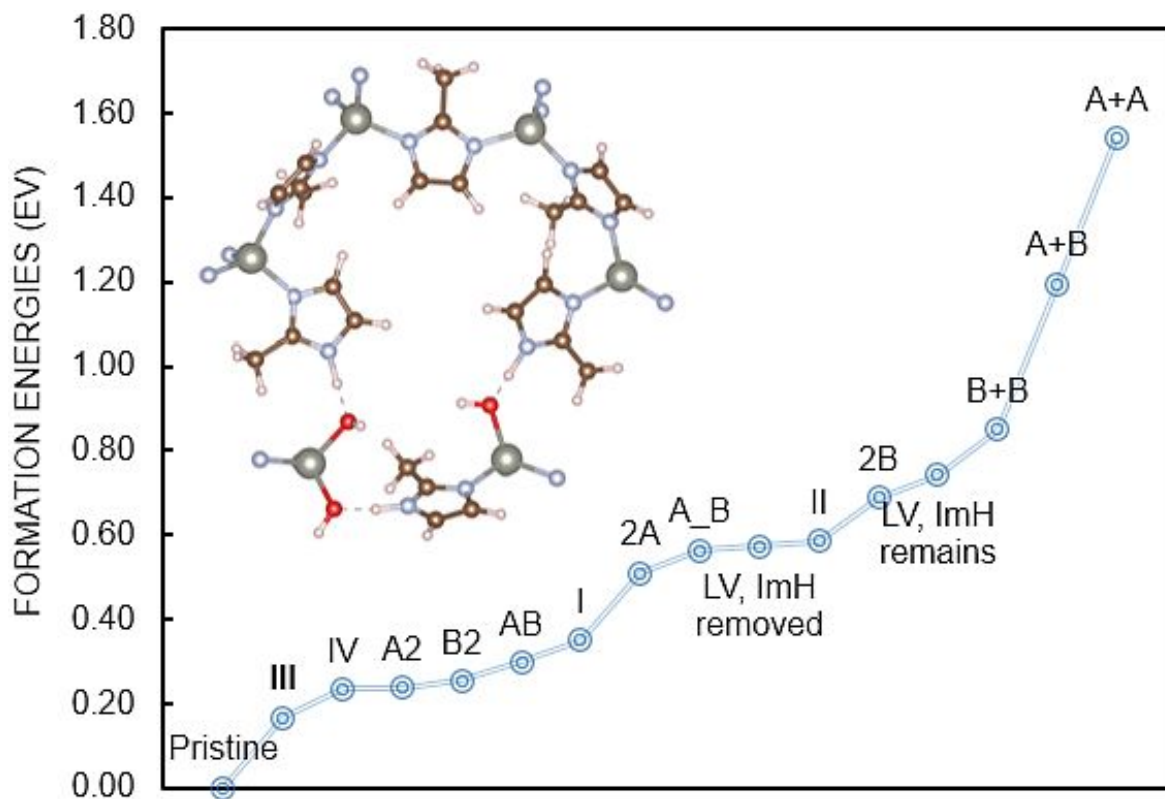


**Figure 12.** Formation energies of ZIF-8 systems with two and three defects, referenced to the pristine ZIF-8 structure. The defect triplets from Figure 11 are labelled I, II, III and IV. The defect triplet labelled III (see Figure 11) is the most stable structure and its geometry is shown in the inset figure. III and IV both demonstrate examples of triple defect states with lower overall formation energy than any other defect structure. New energies for the defect triplet states are given in Table S3 of the SI.

If we were to extend the above procedure, our data seems to suggest that we could identify energetically favorable states with four defects, five defects, and so on, ultimately leading to amorphization. However, it is worth noting that we have not considered entropic contributions to the defect formation process. In particular, we expect a significant increase in conformational entropy as we add more dangling linkers to the structure. At the same time, since our calculations assume that the proton-donating agent is adsorbing from the gas phase, there is a non-trivial loss of entropy associated with each adsorption event (this is less significant if the proton donor is in the solution phase). A comprehensive investigation of defect propagation must assess the entropy and free energy of the system, which is beyond the scope of the present work.

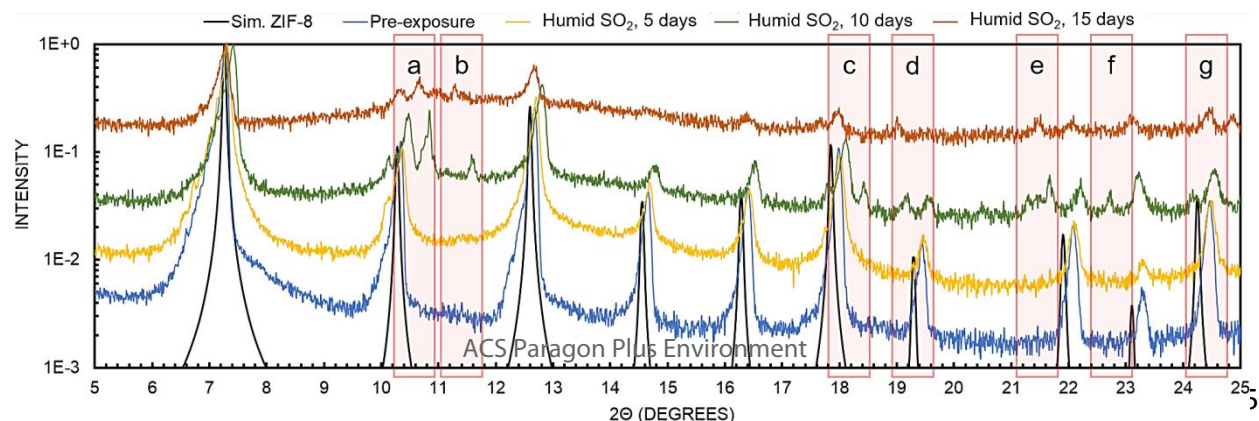
## 4. Discussion

### 4.1. Diffraction patterns of defective materials

The results above provide compelling evidence that formation of point defects in ZIF-8 can be self-propagating in the sense that the presence of initial defects favors the formation of additional nearby defects. It is useful to consider whether this description of defect formation can be readily connected with experimental observations of degraded materials. We have made an initial attempt to tackle this challenging task by comparing the simulated powder pattern for various models of defective materials with experimental X-ray diffraction (XRD) measurements of ZIF-8 exposed to corrosive environments.

Figure 13 shows experimental PXRD spectra from previous work by Bhattacharyya et al. for ZIF-8 exposed to 20 ppm of humid  $\text{SO}_2$  for 5, 10, and 15 days, with each spectrum normalized to the highest intensity peak.<sup>17</sup> A simulated powder pattern for pristine ZIF-8 is shown for reference. Degradation of the material is associated with loss of peak intensity, an increase in broad amorphous background, changes in peak position, and the appearance of peak splitting or new peaks. The main changes in peak position are highlighted in

Figure 13 (labelled a-g) and they are most pronounced in the spectra taken after 10 days of exposure. After 15 days of exposure, the BET surface area of the material had decreased by 55% relative to the pre-exposed material and the crystallinity relative to the sample after 10 days of exposure was reduced.



1  
2  
3 **Figure 13.** Experimental XRD spectra of ZIF-8 after exposure to humid SO<sub>2</sub> for 0, 5, 10, and 15 days, with the  
4 simulated powder pattern of pristine ZIF-8 shown for comparison. Each spectrum has been normalized to the  
5 highest peak intensity and no offsets were used in plotting the spectra. The main instances of peak splitting and  
6 new peaks are highlighted in red and labelled a-g. Experimental data was obtained from Bhattacharyya et al.<sup>11</sup>  
7

8         When considering whether models of defective structures might give insight into the  
9 experimental spectra, we can identify two extremes; one where isolated defects are spread  
10 throughout the material, and one where we have a clustered pocket of defects in an otherwise  
11 pristine material. Our earlier predictions about defect clustering behavior would suggest the latter  
12 is more likely to occur, especially in earlier stages of degradation.  
13  
14  
15  
16  
17  
18

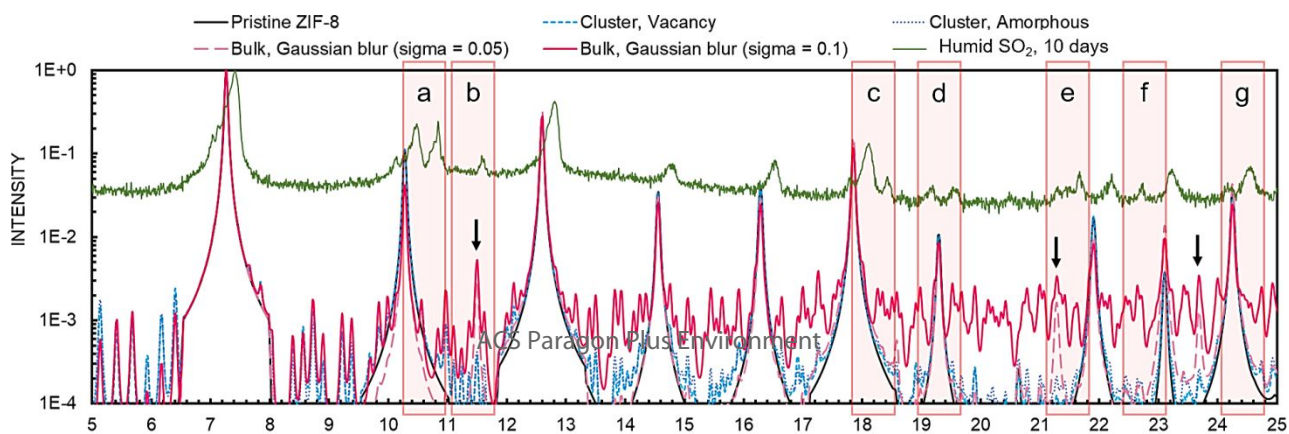
19         To model the clustered defects, we considered two cases representing degradation  
20 restricted to a pocket of defects. We defined the simulation models by constructing 3×3×3  
21 superlattices and introducing defects only in one 1×1×1 cell. In one case, all the linkers in the  
22 defect pocket were cleaved from the Zn framework and removed, creating a vacant defect  
23 pocket. This was approximated by a 3×3×3 simulation volume with all the atoms in one unit cell  
24 removed. In the second case, we considered a system where all the linkers in the defect pocket  
25 have been cleaved and the pocket subsequently collapses into a dense, amorphous phase. This  
26 amorphous pocket was represented by a 3×3×3 simulation model with all the atoms in one  
27 17×17×17 Å<sup>3</sup> unit cell randomly moved to new positions within a 14×14×14 Å<sup>3</sup> volume centered  
28 within the unit cell. In both cases, we broke all 48 Zn-N out of a total 1,296 Zn-N bonds in the  
29 3×3×3 superlattice, giving a defect concentration of 3.7% calculated in terms of the number of  
30 Zn-N bonds. Clearly neither of these simple models accurately represents the atomic structure of  
31 a fully evolved cluster of defects, but they can provide some initial intuition. Figure 14 shows  
32 simulated XRD spectra for the vacated (blue dashed line) and amorphous (blue dotted line)  
33 defect pockets. In both cases, the minor changes that appear in the spectra are not similar to what  
34 is seen experimentally. This suggests that while it seems likely that defect “pockets” can appear  
35  
36  
37  
38  
39  
40  
41  
42  
43  
44  
45  
46  
47  
48  
49  
50  
51  
52  
53  
54  
55  
56  
57  
58  
59  
60

1  
2  
3 in the initial stages of degradation, these structures will not have a simple experimental signature  
4  
5 accessible by powder XRD.  
6

7  
8 To model materials with spatially separated defects, we started by randomly inserted one  
9  
10 dangling-linker defect per unit cell in a  $1\times 1\times 1$  superlattice. Breaking one Zn-N bond out of 48  
11  
12 total bonds in every unit cell gives a 4.1% defect concentration. Unlike the clustered defect  
13  
14 model, however, the simulated spectra of the 1 defect/cell bulk structure (see Figure S4 in the SI)  
15  
16 showed a sharp increase in background signal. Many of these new peaks are likely to be artefacts  
17  
18 related to the specific periodicity of our simulation. To distinguish the new features that are  
19  
20 caused by defects, we constructed additional  $2\times 2\times 2$  and  $5\times 5\times 4$  superlattices with 1 dangling  
21  
22 linker defect independently inserted at random in each unit cell. The XRD simulated spectra for  
23  
24 these models (see Figure S5 in the SI) **Error! Reference source not found.** showed variation in  
25  
26 the amount of background signal. Unsurprisingly, the largest simulation volume ( $5\times 5\times 4$   
27  
28 superlattice) most closely approximates a macroscopic bulk structure, showing background most  
29  
30 similar to the background broadening we measure experimentally. Several peaks consistent  
31  
32 across varying simulation size are indicated by black arrows in Figure S5. We also tested  
33  
34 sensitivity to the overall concentration of defects by building models where we randomly  
35  
36 introduced 1 dangling linker defect per  $1\times 1\times 1$  unit cell, 1 defect per 2 unit cells (0.5  
37  
38 defects/cell), or 1 defect per 3 unit cells (0.3 defects/cell) into a  $3\times 3\times 3$  superlattice. Reducing the  
39  
40 defect concentration to 0.3 defects/cell significantly reduces background noise in the simulated  
41  
42 XRD spectrum (see Figure S6 in the SI), but we find that three of the new peaks consistent  
43  
44 across simulation size are also robust to the defect concentration, as indicated by black arrows in  
45  
46 Figure S6. These peaks occur at approximately  $11.5^\circ$ ,  $21.3^\circ$  and  $23.7^\circ$ , corresponding to  
47  
48  
49  
50  
51  
52  
53  
54  
55  
56  
57  
58  
59  
60

1  
2  
3 diffraction from the  $(6\ 0\ \bar{3})$ ,  $(12\ 0\ 3)$ , and  $(12\ 6\ 3)$  lattice planes, respectively. The reason that  
4  
5 these particular high index lattice planes appear is not obvious to us.  
6  
7

8 Finally, we modeled a “severely degraded” limit of high defect concentration. Since  
9  
10 experiments have shown that degraded ZIF-8 can be recovered to its pristine state through  
11  
12 immersion in a linker-rich solution<sup>21</sup>, we constructed two examples of this degraded state by  
13  
14 adding to all atomic positions in a  $3\times 3\times 3$  superlattice a random shift drawn from a Gaussian  
15  
16 distribution with mean  $\mu = 0\ \text{\AA}$  and standard deviation  $\sigma = 0.05\ \text{\AA}$  (Figure 14, dashed red line) or  
17  
18  $\sigma = 0.1\ \text{\AA}$  (Figure 14, solid red line) in three dimensions. Although these structures are not easily  
19  
20 recognized as ZIF-8, they retain similar long-range periodicity to the pristine state, seen in the  
21  
22 consistency of the major peaks. We can compare them to the experimentally exposed material  
23  
24 (Figure 14, green line) as well as the main changes in peak position previously identified for the  
25  
26 degraded structure. Significant blurring of the atomic positions ( $\sigma = 0.1\ \text{\AA}$ ) is necessary to  
27  
28 produce amorphous background comparable to that seen in experimental spectra for degraded  
29  
30 ZIF-8; the bulk model with only slight blurring has negligible background. While there are  
31  
32 features in this model that resemble features attributed to defects in the experimental degraded  
33  
34 structure, they are not sufficiently distinguishable from the overall background noise. However,  
35  
36 it is interesting to note that the same peaks identified earlier at  $11.5^\circ$ ,  $21.3^\circ$  and  $23.7^\circ$  are present  
37  
38 (Figure 14, black arrows) in both bulk defect models with slight blurring and significant blurring  
39  
40 of the atomic positions. Additionally, the peaks at  $11.5^\circ$  and  $21.3^\circ$  may match experimental  
41  
42 features b and e.  
43  
44  
45  
46  
47  
48  
49



1  
2  
3 **Figure 14.** Simulated XRD patterns of ZIF-8 where defects are clustered in a single cell of a  $3\times 3\times 3$  superlattice (blue, short dashed and dotted), and where the bulk of the  $3\times 3\times 3$  superlattice is degraded (red, dashed and solid). The clustered defect structures and slightly degraded bulk structure (red, dashed) show little change from the pristine ZIF-8 spectra, but the severely degraded structure (red, solid) shows significant increase in amorphous background and new peaks (black arrows). Experimental data of ZIF-8 exposed to 20 ppm of humid  $\text{SO}_2$  for 10 days is shown in green (from Figure 13), with the same peak splitting and new peak features highlighted as from Figure 13. All spectra are normalized to their highest peak.

10  
11 We have identified defect models where the simulated power patterns are comparable to  
12 the experimental XRD spectra of degraded ZIF-8 structures in increased background noise and  
13 new peaks. The intensity and broadness of background noise are dependent on system size, but  
14 the new peaks around  $11.5^\circ$  and  $21.3^\circ$  are consistent even when we vary the system size ( $2\times 2\times 2$ ,  
15  $3\times 3\times 3$ , or  $5\times 5\times 4$  systems), defect concentration (1 defect/cell, 0.5 defects/cell, and 0.3  
16 defects/cell), and type of defect (dangling linker, or Gaussian blurred). This suggests that even  
17 though powder XRD is a spatially averaged technique, there may be some signatures of local  
18 degradation of ZIF-8 that are detectable using XRD.

## 31 5. Conclusion

32  
33  
34 In this paper, we have focused on the sequence of events that ultimately leads to  
35 degradation of ZIF-8, a prototypical MOF, in the presence of adsorbed water or humid acid  
36 gases. Using DFT calculations, we considered a wide range of scenarios for forming single or  
37 pair defect states in ZIF-8. We demonstrated that defect proximity reduces the formation energy  
38 of the second defect in a pair of defects. We also showed that the formation energy can be further  
39 reduced when a third defect is added in close proximity to an existing pair of defects. These  
40 observations strongly suggest the spontaneous formation of clusters of defects in ZIF-8 is likely  
41 in any situation where initial formation of isolated point defects will occur. In the case of defect  
42 pairs, adjacent and co-terminally located defects are favored. Among the limited set of defect  
43 triplets we considered, the most energetically preferred states place the defects in 6M rings of  
44  
45  
46  
47  
48  
49  
50  
51  
52  
53  
54  
55  
56  
57  
58  
59  
60

1  
2  
3 ZIF-8 where the larger ring size can more flexibly accommodate them. A simple description that  
4 approximates the defect formation energy as the sum of an intrinsic bond-breaking cost that is  
5 independent of defect type or clustering and a strain cost associated with the local geometry and  
6 conformation around the defect site is a useful way to understand our results. This is a  
7 mechanism that is likely not restricted to ZIF-8 defects; it seems likely that a similar description  
8 will be helpful in assessing the preference for defect clustering in other MOFs.  
9

10  
11 Our DFT calculations have only examined the thermodynamics of defect clustering. The  
12 energetic preference for defect clustering suggests it is plausible that the activation energies for  
13 creating new defects adjacent to existing defects are lower than for creating isolated defects, but  
14 we have not directly tested this hypothesis. We also cannot conclusively state that the energetic  
15 preference for defect clustering continues as the defect clusters continue to increase in size. The  
16 description given above in terms of strain relaxation hints that defect clustering is unlikely to  
17 self-terminate, but we cannot categorically rule out the possibility that configurations of more  
18 than three defects exist for which the strain cost of adding additional defects increases with  
19 cluster size.  
20  
21

22  
23 Finally, we qualitatively considered how our calculations, which focused on water-  
24 induced defects, relate to experimentally observed degradation of ZIF-8 in the presence of humid  
25 SO<sub>2</sub>. Our DFT calculations compared the energetics of defect propagation when we substitute  
26 water in our models with sulfuric acid and found that partial substitution results in a much more  
27 favorable degradation reaction, in agreement with the experimental observation that humid SO<sub>2</sub>  
28 degrades ZIF-8 much more severely than humidity alone. Second, we constructed a variety of  
29 defect models and compared the simulated powder patterns against experimental XRD spectra  
30 for degraded ZIF-8. We find new peaks around 11.5°, 21.3°, and 23.7° robust to variation of  
31  
32  
33  
34  
35  
36  
37  
38  
39  
40  
41  
42  
43  
44  
45  
46  
47  
48  
49  
50  
51  
52  
53  
54  
55  
56  
57  
58  
59  
60

1  
2  
3 system size, defect concentration, and defect type; these peaks are likely indicative of defect  
4 presence and may match new features observed in the experimentally degraded structure.  
5  
6  
7  
8  
9

### 10 **Supporting Information:**

11  
12 Formation energies for all defect structures discussed; additional site vacancy energetics for two  
13 and three defect states; structure files containing optimized lattice vectors and atomic positions  
14 for all defect structures; structure files containing lattice vectors and atomic positions for  
15 superlattice models; additional simulated XRD patterns of superlattice models; intensity and two  
16 theta data for all experimental and simulated XRD patterns  
17  
18  
19  
20  
21  
22  
23  
24  
25

### 26 **Notes**

27  
28 The authors declare no competing financial interest.  
29  
30  
31  
32

### 33 **Acknowledgments**

34  
35 This work was supported as part of UNCAGE-ME, an Energy Frontier Research Center funded  
36 by the U.S. Department of Energy, Office of Science, Basic Energy Sciences under Award # DE-  
37 SC0012577. This work used the Extreme Science and Engineering Discovery Environment  
38 (XSEDE) *Stampede 2* at the *Texas Advanced Computer Center* through allocation TG-  
39 CHE120088.  
40  
41  
42  
43  
44  
45  
46  
47  
48  
49  
50  
51  
52  
53  
54  
55  
56  
57  
58  
59  
60

## References

1. Banerjee, R.; Phan, A.; Wang, B.; Knobler, C.; Furukawa, H.; O'Keeffe, M.; Yaghi, O. M., High-Throughput Synthesis of Zeolitic Imidazolate Frameworks and Application to CO<sub>2</sub> Capture. *Science* **2008**, *319*, 939-943.
2. Sholl, D. S.; Lively, R. P., Seven Chemical Separations to Change the World. *Nature* **2016**, *532*, 435-437.
3. Keskin, S.; van Heest, T. M.; Sholl, D. S., Can Metal-Organic Framework Materials Play a Useful Role in Large-Scale Carbon Dioxide Separations? *Chem. Sus. Chem.* **2010**, *3*, 879-91.
4. Howarth, A. J.; Liu, Y.; Li, P.; Li, Z.; Wang, T. C.; Hupp, J. T.; Farha, O. K., Chemical, Thermal and Mechanical Stabilities of Metal–Organic Frameworks. *Nat. Rev. Mater.* **2016**, *1*, 15018.
5. Zhou, K.; Mousavi, B.; Luo, Z.; Phatanasri, S.; Chaemchuen, S.; Verpoort, F., Characterization and Properties of Zn/Co Zeolitic Imidazolate Frameworks Vs. ZIF-8 and ZIF-67. *J. Mater. Chem. A* **2017**, *5*, 952-957.
6. Walton, K. S.; Sholl, D. S., Research Challenges in Avoiding “Showstoppers” in Developing Materials for Large-Scale Energy Applications. *Joule* **2017**, *1*, 208-211.
7. Park, K. S.; Ni, Z.; Cote, A. P.; Choi, J. Y.; Huang, R.; Uribe-Romo, F. J.; Chae, H. K.; O'Keeffe, M.; Yaghi, O. M., Exceptional Chemical and Thermal Stability of Zeolitic Imidazolate Frameworks. *Proc. Natl. Acad. Sci. U. S. A.* **2006**, *103*, 10186-91.
8. Küsgens, P.; Rose, M.; Senkovska, I.; Fröde, H.; Henschel, A.; Siegle, S.; Kaskel, S., Characterization of Metal-Organic Frameworks by Water Adsorption. *Micropor. Mesopor. Mater.* **2009**, *120*, 325-330.
9. Burtch, N. C.; Jasuja, H.; Walton, K. S., Water Stability and Adsorption in Metal-Organic Frameworks. *Chem. Rev.* **2014**, *114*, 10575-612.
10. Liu, D.; Ma, X.; Xi, H.; Lin, Y. S., Gas Transport Properties and Propylene/Propane Separation Characteristics of ZIF-8 Membranes. *J. Memb. Sci.* **2014**, *451*, 85-93.
11. Liu, X.; Li, Y.; Ban, Y.; Peng, Y.; Jin, H.; Bux, H.; Xu, L.; Caro, J.; Yang, W., Improvement of Hydrothermal Stability of Zeolitic Imidazolate Frameworks. *Chem. Commun.* **2013**, *49*, 9140-9142.
12. Zhang, H.; Liu, D.; Yao, Y.; Zhang, B.; Lin, Y. S., Stability of ZIF-8 Membranes and Crystalline Powders in Water at Room Temperature. *J. Memb. Sci.* **2015**, *485*, 103-111.
13. Sholl, D. S.; Lively, R. P., Defects in Metal-Organic Frameworks: Challenge or Opportunity? *J. Phys. Chem. Lett* **2015**, 3437-3444.
14. Zhang, C.; Han, C.; Sholl, D. S.; Schmidt, J. R., Computational Characterization of Defects in Metal-Organic Frameworks: Spontaneous and Water-Induced Point Defects in ZIF-8. *J. Phys. Chem. Lett* **2016**, *7*, 459-64.
15. Han, C.; Zhang, C.; Tymieńska, N.; Schmidt, J. R.; Sholl, D. S., Insights Into the Stability of Zeolitic Imidazolate Frameworks in Humid Acidic Environments from First-Principles Calculations. *J. Phys. Chem. C* **2018**, *122*, 4339-4348.
16. Han, C.; Verploegh, R. J.; Sholl, D. S., Assessing the Impact of Point Defects on Molecular Diffusion in ZIF-8 Using Molecular Simulations. *J. Phys. Chem. Lett* **2018**, *9*, 4037-4044.
17. Bhattacharyya, S.; Han, R.; Kim, W.-G.; Chiang, Y.; Jayachandrababu, K. C.; Hungerford, J. T.; Dutzer, M. R.; Ma, C.; Walton, K. S.; Sholl, D. S.; Nair, S., Acid Gas Stability

of Zeolitic Imidazolate Frameworks: Generalized Kinetic and Thermodynamic Characteristics. *Chem. Mater.* **2018**, *30*, 4089-4101.

18. Kwon, H. T.; Jeong, H.-K.; Lee, A. S.; An, H. S.; Lee, T.; Jang, E.; Lee, J. S.; Choi, J., Defect-Induced Ripening of Zeolitic-Imidazolate Framework ZIF-8 and Its Implication to Vapor-Phase Membrane Synthesis. *Chem. Commun.* **2016**, *52*, 11669-11672.

19. Lee, M. J.; Kwon, H. T.; Jeong, H.-K., Defect-Dependent Stability of Highly Propylene-Selective Zeolitic-Imidazolate Framework ZIF-8 Membranes. *J. Memb. Sci.* **2017**, *529*, 105-113.

20. Bhattacharyya, S.; Han, R.; Joshi, J.; Zhu, G.; Lively, R. P.; Walton, K. S.; Sholl, D. S.; Nair, S., NO<sub>2</sub> Stability of Zeolitic Imidazolate Frameworks. *J. Phys. Chem. C* **2018**, *123*, 2336-2346.

21. Jayachandrababu, K. C.; Bhattacharyya, S.; Chiang, Y.; Sholl, D. S.; Nair, S., Recovery of Acid-Gas-Degraded Zeolitic Imidazolate Frameworks by Solvent-Assisted Crystal Redemption (SACRed). *ACS Appl. Mater. Interfaces* **2017**, *9*, 34597-34602.

22. Leus, K.; Bogaerts, T.; De Decker, J.; Depauw, H.; Hendrickx, K.; Vrielinck, H.; Van Speybroeck, V.; Van Der Voort, P., Systematic Study of the Chemical and Hydrothermal Stability of Selected “Stable” Metal Organic Frameworks. *Micropor. Mesopor. Mater.* **2016**, *226*, 110-116.

23. Pang, S. H.; Han, C.; Sholl, D. S.; Jones, C. W.; Lively, R. P., Facet-Specific Stability of ZIF-8 in the Presence of Acid Gases Dissolved in Aqueous Solutions. *Chem. Mater.* **2016**, *28*, 6960-6967.

24. Ling, S.; Slater, B., Dynamic Acidity in Defective UiO-66. *Chem. Sci.* **2016**, *7*, 4706-4712.

25. Wu, H.; Chua, Y. S.; Krungleviciute, V.; Tyagi, M.; Chen, P.; Yildirim, T.; Zhou, W., Unusual and Highly Tunable Missing-Linker Defects in Zirconium Metal-Organic Framework UiO-66 and Their Important Effects on Gas Adsorption. *J. Am. Chem. Soc.* **2013**, *135*, 10525-32.

26. Cliffe, M. J.; Wan, W.; Zou, X.; Chater, P. A.; Kleppe, A. K.; Tucker, M. G.; Wilhelm, H.; Funnell, N. P.; Coudert, F.-X.; Goodwin, A. L., Correlated Defect Nanoregions in a Metal-Organic Framework. *Nat. Commun.* **2014**, *5*, 4176.

27. Goodenough, J. B., Influence of Atomic Vacancies on the Properties of Transition-Metal Oxides. I. TiO<sub>x</sub> and VO<sub>x</sub>. *Phys. Rev. B* **1972**, *5*, 2764-2774.

28. Burdett, J. K.; Mitchell, J. F., Nonstoichiometry in Early Transition Metal Compounds with the Rocksalt Structure. *Prog Solid State Chem* **1995**, *23*, 131-170.

29. Gupta, F.; Brillant, G.; Pasturel, A., Correlation Effects and Energetics of Point Defects in Uranium Dioxide: A First Principle Investigation. *Philos. Mag.* **2007**, *87*, 2561-2569.

30. Alfè, D.; Gillan, M. J., Schottky Defect Formation Energy in MgO Calculated by Diffusion Monte Carlo. *Phys. Rev. B* **2005**, *71*, 220101.

31. Bristow, J. K.; Svane, K. L.; Tiana, D.; Skelton, J. M.; Gale, J. D.; Walsh, A., Free Energy of Ligand Removal in the Metal-Organic Framework UiO-66. *J. Phys. Chem. C* **2016**, *120*, 9276-9281.

32. Swaminathan, N.; Morgan, D.; Szlufarska, I., Ab Initio Based Rate Theory Model of Radiation Induced Amorphization in B-SiC. *J. Nucl. Mater.* **2011**, *414*, 431-439.

33. Tyburska-Püschel, B.; Zhai, Y.; He, L.; Liu, C.; Boulle, A.; Voyles, P. M.; Szlufarska, I.; Sridharan, K., Size Distribution of Black Spot Defects and Their Contribution to Swelling in Irradiated SiC. *J. Nucl. Mater.* **2016**, *476*, 132-139.

- 1  
2  
3 34. Liu, C.; He, L.; Zhai, Y.; Tyburska-Püschel, B.; Voyles, P. M.; Sridharan, K.; Morgan,  
4 D.; Szlufarska, I., Evolution of Small Defect Clusters in Ion-Irradiated 3C-SiC: Combined  
5 Cluster Dynamics Modeling and Experimental Study. *Acta Mater.* **2017**, *125*, 377-389.  
6  
7 35. Perdew, J. P.; Burke, K.; Ernzerhof, M., Generalized Gradient Approximation Made  
8 Simple. *Phys. Rev. Lett.* **1996**, *77*, 3865-3868.  
9  
10 36. Grimme, S.; Antony, J.; Ehrlich, S.; Krieg, H., A Consistent and Accurate Ab Initio  
11 Parametrization of Density Functional Dispersion Correction (DFT-D) for the 94 Elements H-Pu.  
12 *J. Chem. Phys.* **2010**, *132*, 154104.  
13  
14 37. De Vita, A.; Gillan, M. J.; Lin, J. S.; Payne, M. C.; Štich, I.; Clarke, L. J., Defect  
15 Energetics in MgO Treated by First-Principles Methods. *Phys. Rev. B* **1992**, *46*, 12964-12973.  
16  
17 38. The CP2K developers group, 2013. CP2K is freely available from <http://www.cp2k.org/>  
18 (accessed May 15, 2013)..  
19  
20 39. VandeVondele, J.; Krack, M.; Mohamed, F.; Parrinello, M.; Chassaing, T.; Hutter, J.,  
21 Quickstep: Fast and Accurate Density Functional Calculations Using a Mixed Gaussian and  
22 Plane Waves Approach. *Comput. Phys. Commun.* **2005**, *167*, 103-128.  
23  
24 40. Krack, M.; Parrinello, M. *Quickstep: Make the Atoms Dance*; John von Neumann  
25 Institute for Computing: Jülich, Germany, 2005; pp 29-51.  
26  
27 41. Goedecker, S.; Teter, M.; Hutter, J., Separable Dual-Space Gaussian Pseudopotentials.  
28 *Phys. Rev. B* **1996**, *54*, 1703-1710.  
29  
30 42. Hartwigsen, C.; Goedecker, S.; Hutter, J., Relativistic Separable Dual-Space Gaussian  
31 Pseudopotentials from H to Rn. *Phys. Rev. B* **1998**, *58*, 3641-3662.  
32  
33 43. Krack, M., Pseudopotentials for H to Kr Optimized for Gradient-Corrected Exchange-  
34 Correlation Functionals. *Theor. Chem. Acc.* **2005**, *114*, 145-152.  
35  
36 44. VandeVondele, J.; Hutter, J., Gaussian Basis Sets for Accurate Calculations on Molecular  
37 Systems in Gas and Condensed Phases. *J. Chem. Phys.* **2007**, *127*, 114105.  
38  
39 45. Lippert, B. G.; Parrinello, J. H.; Michele, A Hybrid Gaussian and Plane Wave Density  
40 Functional Scheme. *Mol. Phys.* **1997**, *92*, 477-488.  
41  
42 46. Macrae, C. F.; Bruno, I. J.; Chisholm, J. A.; Edgington, P. R.; McCabe, P.; Pidcock, E.;  
43 Rodriguez-Monge, L.; Taylor, R.; van de Streek, J.; Wood, P. A., Mercury CSD 2.0– New  
44 Features for the Visualization and Investigation of Crystal Structures. *J. Appl. Crystallogr.* **2008**,  
45 *41*, 466-470.  
46  
47 47. Momma, K.; Izumi, F., VESTA 3 for Three-Dimensional Visualization of Crystal,  
48 Volumetric and Morphology Data. *J. Appl. Crystallogr.* **2011**, *44*, 1272-1276.  
49  
50  
51  
52  
53  
54  
55  
56  
57  
58  
59  
60

## TOC Graphic

